Supporting online material: Observations of Saturn's magnetospheric cusp

J. M. Jasinski,[1,2] C. S. Arridge,[1,2] L. Lamy,[3] J. S. Leisner,[4] M. F. Thomsen,[5]
D. G. Mitchell,[6] A. J. Coates,[1,2] A. Radioti,[7] G. H. Jones,[1,2] E. Roussos,[8]
N.Krupp,[8] D. Grodent,[7] M. K. Dougherty,[5] and J. H. Waite[9]

[1]Mullard Space Science Laboratory, University College London, UK.

[2]The Centre for Planetary Sciences at UCL/Birkbeck, London, UK.

[3]LESIA, Observatoire de Paris, Université Paris Diderot, France.

[4]Blackett Laboratory, Imperial College London, UK.

[5]Planetary Science Institute, Tucson, Arizona, USA.

[6]Applied Physics Laboratory, Johns Hopkins University, Laurel, Maryland, USA.

[7]Université de Liége, Liege, Belgium.

[8]Max-Planck-Institut für Sonnensystemforschung, Göttingen, Germany.

[9]Southwest Research Institute, San Antonio, Texas, USA.

In this online supporting material, we present some of the methods and analysis not included in the main paper submitted to GRL.

1. Instrumentation

Four of the six suites of in situ instruments located onboard Cassini are used for the analysis in this paper: the Cassini Plasma Spectrometer (CAPS), Dual Technique Magnetometer (MAG), Magnetospheric Imaging Instrument (MIMI), and Radio & Plasma Wave Science (RPWS).

The data from the following instruments were used: the Electron Spectrometer (ELS) and Ion Mass Spectrometer (IMS) from CAPS [*Young et al.*, 2004]; the low energy magnetospheric measurements system (LEMMS) from MIMI [*Krimigis et al.*, 2004]; the MAG instrument [*Dougherty et al.*, 2004]; and the Low, Medium and High Frequency Receivers (LFR, MFR, and HFR) of the Radio Plasma Wave Science (RPWS) instrument [*Gurnett et al.*, 2004]. We also present auroral data from the Ultraviolet Imaging Spectrograph (UVIS) onboard Cassini [*Esposito et al.*, 2004].

To complete the picture of the solar wind upstream conditions at Saturn, we present model heliospheric data at Saturn (ENLIL) produced by Community Coordinated Modeling Center (CCMC), to accompany interpretation of the Saturn Kilometric data (SKR) from RPWS.

2. Observations

Figure A shows the KSM X-Z projection of the trajectory of the Cassini spacecraft during these observations. The Sun is to the right and the view is from dawn. The section of the trajectory highlighted in red shows the part of the trajectory where we observe the cusp. We can see that Cassini is travelling in a poleward trajectory and observes the cusp in the high latitudes.

The ions observed in what we identify as the cusp (~1100-1900 UT) have a mass composition entirely consistent with a solar wind origin. We base this conclusion on the following arguments:

1) From ~1100 to ~1400 UT, the spacecraft was rolling, so the CAPS field of view covered the full sky, with a period of ~30 minutes. Throughout this whole interval, the CAPS SNG ion data show a steady population with a single peak between ~200 eV and ~2 keV (Figure 1 of main paper). While there is some weak modulation with actuation and roll during this interval, there is no hidden ion population that only shows up at some special look direction.

2) Between 1100 and 1400 UT, CAPS obtained 6 time-of-flight (TOF) accumulations, each covering 512 seconds, and phased by ~60 degrees from one accumulation to the next. Hence, we have TOF coverage over essentially the full sky. TOF measurements between 1100 and 1400 show zero W^+ ions; rather, there are substantial numbers of counts in H^+ and m/q=2 (either He^{++} if the plasma is of solar wind origin, or H^{2+} if it is of magnetospheric origin [e.g., *Thomsen et al.*, 2010]). The light ion counts cover precisely the energy range of the single peak observed persistently in the SNG data. If the TOF accumulation is extended to cover the entire time range from 1100 to 1800 UT, we still find zero W^+ counts. There are some signs of very small amounts of W+ ions present, however they are sporadic and around the 1-count level, such that if any W+ population is present, it is essentially below the threshold for CAPS detectability.

3) In addition to the absence of W^+, the light-ion composition provides a useful signature of the origin of the plasma. In particular, from the few valid numerical moments obtained during the interval 1100-1800 UT (i.e., when the spacecraft was not rolling, basically 1130-1215 and 1400-1800 UT), the derived values of the light ion densities were in the ratio (m/q=2:m/q=1)$\sim$0.01-0.04, entirely consistent with solar wind composition and well below typical values of >0.1 (even up to 1) seen in the outer magnetosphere [e.g., *Thomsen et al.*, 2010]. This can be seen in Figure B. Indeed, in the most recent interval of clearly magnetospheric plasma prior to the cusp interval ($\sim$1900-2000 UT on 20 January), the ratio was $\sim$0.7-0.9. While it might be argued that during the non-rolling intervals from which the cusp moments were obtained the field of view may not have encompassed the main population, similar ratios ($\sim$0.01-0.04) emerge from the integrations done while the spacecraft was rolling as well.

2.1. Estimating the Upstream Conditions

In Figure C we present model heliospheric solar wind conditions at Saturn modelled by ENLIL. ENLIL is a 3D magnetohydrodynamic model of the heliosphere that is time-dependent. It uses and finds the solutions to equations regarding plasma, magnetic field, momentum and energy transport using a Flux-Corrected-Transport algorithm, with initial and boundary conditions based on solar observations [*Odstrcil*, 2003]. The model predicts a modest increase in the velocity, magnetic strength and ram pressure at Saturn leading up to the day of the observations of the cusp, marked with a dashed line.

In Figure D we present high resolution dynamic spectra of RPWS-HFR data between 3.5 and 1500kHz, of the SKR observations [*Lamy et al.*, 2008]. The figure is of the whole day on the 21st of January 2009, with time in hours at the bottom. During the time we have identified as a cusp crossing, there were intense SKR emissions extending to low frequencies (as low as 3.5kHz).

Both the model and the observations of the SKR suggest that the magnetosphere is being compressed making the conditions favourable for the occurrence of dayside reconnection.

2.2. Calculating the field-aligned distance to the reconnection site

When in the cusp, *Burch et al.* [1982] showed that there is a pitch angle energy dispersion in the ion observations. From these dispersions we can calculate the distance to the reconnection site. This can be done using their model equation:

$$E(\alpha_o, t) = \frac{M}{2t^2}\left[\int_{s_i}^{s_o} ds/\sqrt{1 - sin^2\alpha_o(B(s)/B_o)}\right]^2 \quad (1)$$

where ds is arc length along a dipole field line, s_o and s_i are the observation and injection points, M is the particle mass, $B(s)$ is the magnetic field strength along the field line, B_o is the magnetic field strength at the observation point, α_o is the observed pitch angle, and t is the transit time of the particle. The integration is made from the injection point via the mirror point to the point of observation.

B_s is calculated from the *Khurana et al.* [2006] model. A best-fit model dispersion curve is created and compared to the data. The χ^2 value of the comparison between the model and the data is calculated. The model carries a number of iterations to carry out χ^2 minimisation. The best-fit model with the lowest χ^2 is chosen.

References

Burch, J. L., P. H. Reiff, R. A. Heelis, W. B. Hanson, J. D. Winningham, C. Gurgiolo, J. D. Menietti, J. N. Barfield, and R. A. Hoffman (1982), Plasma injection and transport in the mid-altitude polar cusp, *Geophys. Res. Lett., 9*, 921–924, doi: 10.1029/GL009i009p00921.

Dougherty, M. K., S. Kellock, D. J. Southwood, A. Balogh, E. J. Smith, B. T. Tsurutani, B. Gerlach, K.-H. Glassmeier, F. Gleim, C. T. Russell, G. Erdos, F. M. Neubauer, and S. W. H. Cowley (2004), The Cassini Magnetic Field Investigation, *SSR*, *114*, 331–383, doi:10.1007/s11214-004-1432-2.

Esposito, L. W., C. A. Barth, J. E. Colwell, G. M. Lawrence, W. E. McClintock, A. I. F. Stewart, H. U. Keller, A. Korth, H. Lauche, M. C. Festou, A. L. Lane, C. J. Hansen, J. N. Maki, R. A. West, H. Jahn, R. Reulke, K. Warlich, D. E. Shemansky, and Y. L. Yung (2004), The Cassini Ultraviolet Imaging Spectrograph Investigation, *Space Science Reviews*, *115*, 299–361, doi:10.1007/s11214-004-1455-8.

Gurnett, D. A., W. S. Kurth, D. L. Kirchner, G. B. Hospodarsky, T. F. Averkamp, P. Zarka, A. Lecacheux, R. Manning, A. Roux, P. Canu, N. Cornilleau-Wehrlin, P. Galopeau, A. Meyer, R. Boström, G. Gustafsson, J.-E. Wahlund, L. Åhlen, H. O. Rucker, H. P. Ladreiter, W. Macher, L. J. C. Woolliscroft, H. Alleyne, M. L. Kaiser, M. D. Desch, W. M. Farrell, C. C. Harvey, P. Louarn, P. J. Kellogg, K. Goetz, and A. Pedersen (2004), The Cassini Radio and Plasma Wave Investigation, *Space Science Reviews*, *114*, 395–463, doi:10.1007/s11214-004-1434-0.

Hill, T. W., and P. H. Reiff (1977), Evidence of magnetospheric cusp proton acceleration by magnetic merging at the dayside magnetopause, *J. Geophys. Res., 82*, 3623–3628, doi:10.1029/JA082i025p03623.

Khurana, K. K., et al. (2006), A Model of Saturn's Magnetospheric Field Based on Latest Cassini Observations, *Abstract #P44A-01*, presented at 2007 Fall Meeting, AGU, San Francisco, Calif., 10-14 Dec.

Krimigis, S. M., D. G. Mitchell, D. C. Hamilton, S. Livi, J. Dandouras, S. Jaskulek, T. P. Armstrong, J. D. Boldt, A. F. Cheng, G. Gloeckler, J. R. Hayes, K. C. Hsieh, W.-H. Ip, E. P. Keath, E. Kirsch, N. Krupp, L. J. Lanzerotti, R. Lundgren, B. H. Mauk, R. W. McEntire, E. C. Roelof, C. E. Schlemm, B. E. Tossman, B. Wilken, and D. J. Williams (2004), Magnetosphere Imaging Instrument (MIMI) on the Cassini Mission to Saturn/Titan, *Space Science Reviews*, *114*, 233–329, doi:10.1007/s11214-004-1410-8.

Lamy, L., P. Zarka, B. Cecconi, R. Prangé, W. S. Kurth, and D. A. Gurnett (2008), Saturn kilometric radiation: Average and statistical properties, *Journal of Geophysical Research (Space Physics)*, *113*, A07201, doi:10.1029/2007JA012900.

Lockwood, M., and M. F. Smith (1994), Low and middle altitude cusp particle signatures for general magnetopause reconnection rate variations. 1: Theory, *J. Geophys. Res., 99*, 8531–8553, doi:10.1029/93JA03399.

Lockwood, M., T. G. Onsager, C. J. Davis, M. F. Smith, and W. F. Denig (1994), The characteristic of the magnetopause reconnection X-line deduced from low-altitude satellite observations of cusp ions, *Geophys. Res. Lett., 21*, 2757–2760, doi:10.1029/94GL02696.

Odstrcil, D. (2003), Modeling 3-D solar wind structure, *Advances in Space Research*, *32*, 497–506, doi:10.1016/S0273-1177(03)00332-6.

Rosenbauer, H., H. Gruenwaldt, M. D. Montgomery, G. Paschmann, and N. Sckopke (1975), Heos 2 plasma observations in the distant polar magnetosphere - The plasma mantle, *J. Geophys. Res., 80*, 2723–2737, doi:10.1029/JA080i019p02723.

Thomsen, M. F., D. B. Reisenfeld, D. M. Delapp, R. L. Tokar, D. T. Young, F. J. Crary, E. C. Sittler, M. A. McGraw, and J. D. Williams (2010), Survey of ion plasma parameters in Saturn's magnetosphere, *J. Geophys. Res.*, *115*, A10220, doi: 10.1029/2010JA015267.

Young, D. T., J. J. Berthelier, M. Blanc, J. L. Burch, A. J. Coates, R. Goldstein, M. Grande, T. W. Hill, R. E. Johnson, V. Kelha, D. J. McComas, E. C. Sittler, K. R. Svenes, K. Szegö, P. Tanskanen, K. Ahola, D. Anderson, S. Bakshi, R. A. Baragiola, B. L. Barraclough, R. K. Black, S. Bolton, T. Booker, R. Bowman, P. Casey, F. J. Crary, D. Delapp, G. Dirks, N. Eaker, H. Funsten, J. D. Furman, J. T. Gosling, H. Hannula, C. Holmlund, H. Huomo, J. M. Illiano, P. Jensen, M. A. Johnson, D. R. Linder, T. Luntama, S. Maurice, K. P. McCabe, K. Mursula, B. T. Narheim, J. E. Nordholt, A. Preece, J. Rudzki, A. Ruitberg, K. Smith, S. Szalai, M. F. Thomsen, K. Viherkanto, J. Vilppola, T. Vollmer, T. E. Wahl, M. Wüest, T. Ylikorpi, and C. Zinsmeyer (2004), Cassini Plasma Spectrometer Investigation, *Space Science Reviews*, *114*, 1–112, doi: 10.1007/s11214-004-1406-4.

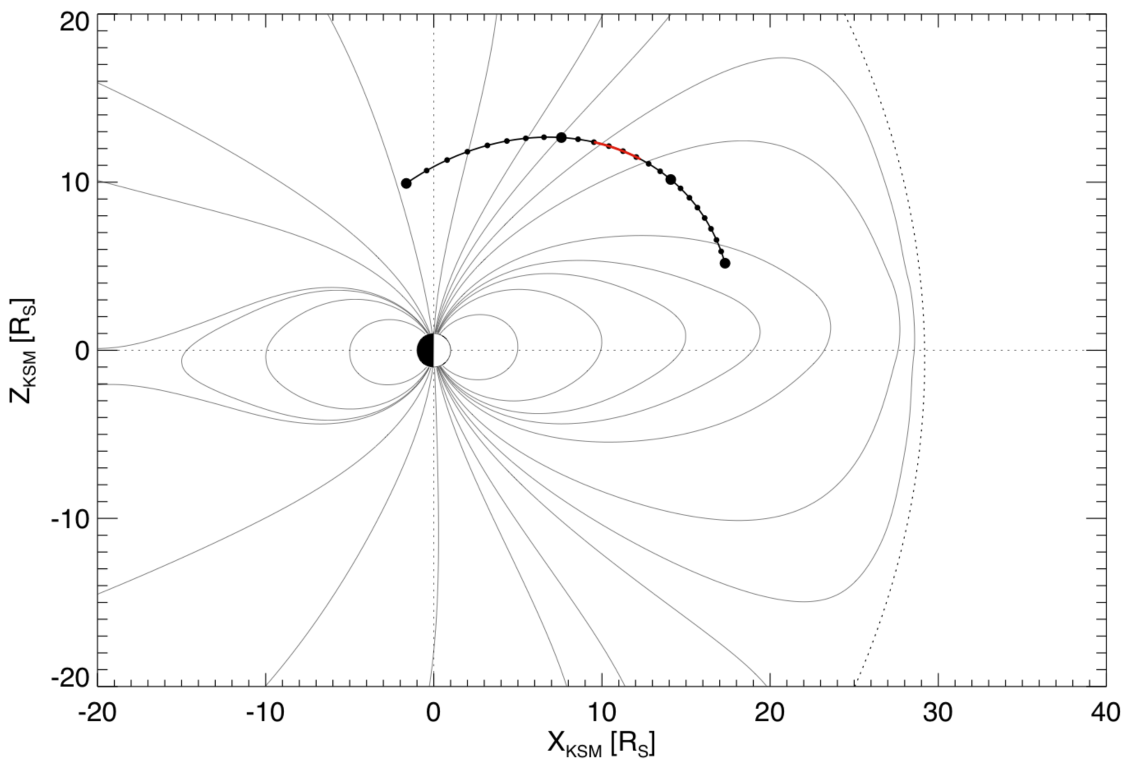

Figure A. Trajectory of Cassini for the 20-22nd January 2009. The figure shows the X-Z projection of the orbit in the Kronocentric-Solar-Magnetospheric (KSM) coordinate system. The Sun is to the right and the view is from dawn. The section of the trajectory highlighted in red shows the part of the trajectory where we observe the cusp. The large dots represent the start of a day in UT, with the closest to the equator being the start of the 20th of January 2009. The smaller dots are separated by three hour intervals. Shown in grey is the Khurana magnetospheric field-line model [*Khurana et al.*, 2006], with the dotted line representing the average position of the magnetopause.

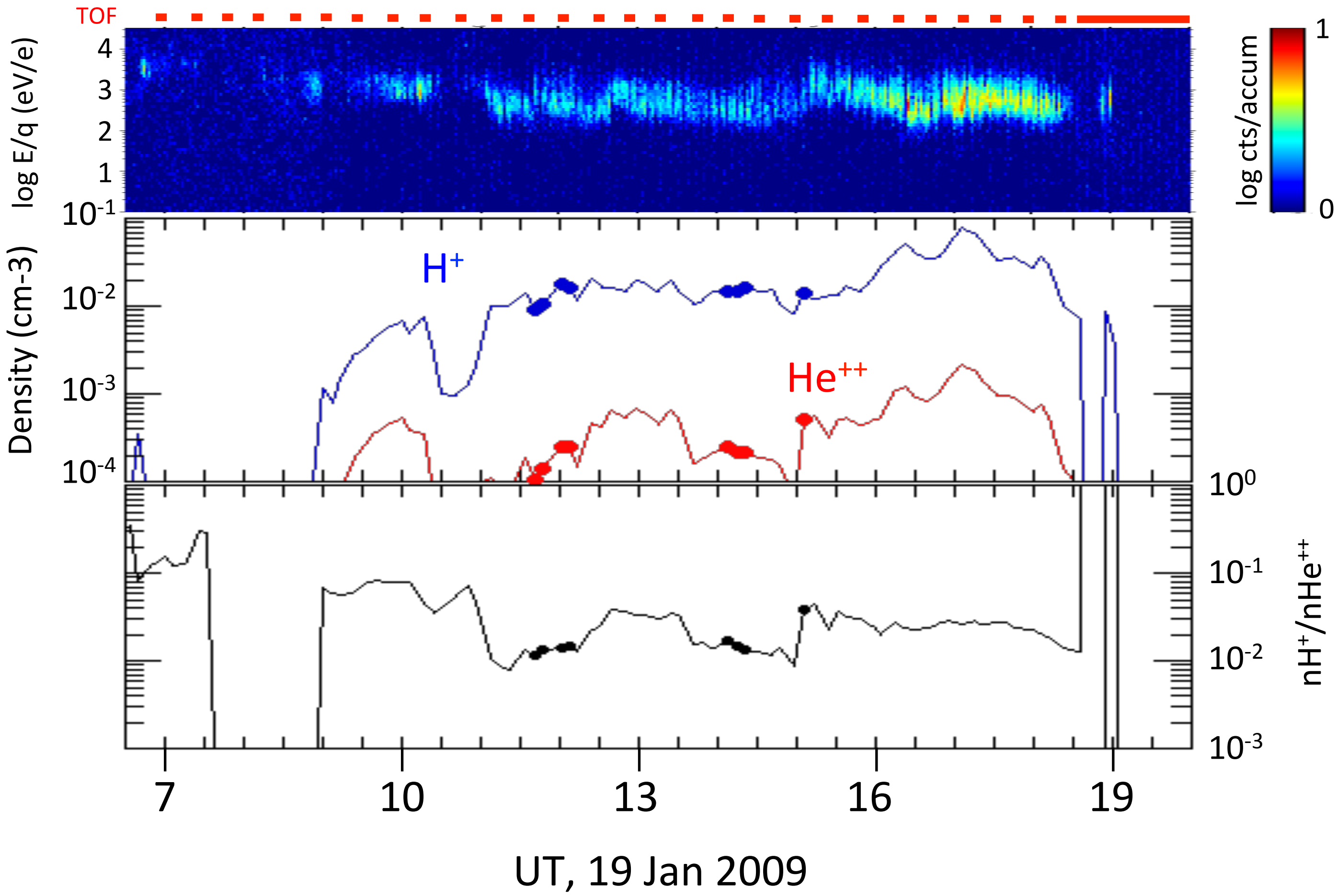

Figure B. Top: Ion spectrogram (all detectors summed together). Middle: light-ion densities. Bottom: the ratio of the m/q=2 to m/q=1 densities. The red bars at the top show the intervals during which time-of-flight (TOF) data were obtained. The ion spectrum does not change radically over this time interval, so we do not expect a change in the TOF data in between the intervals.

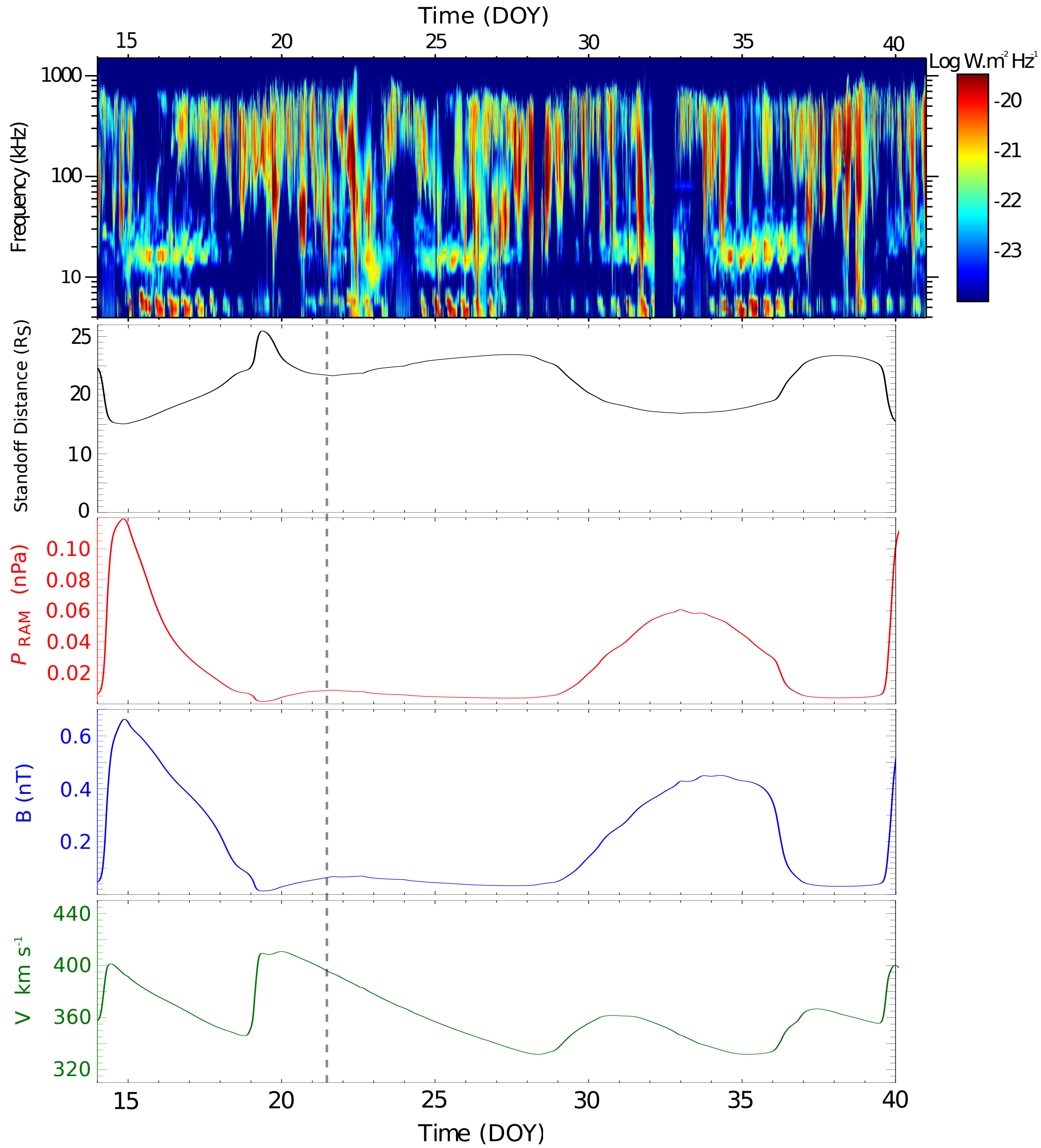

Figure C. Upstream conditions for 14 Jan - 7 Feb 2008. (a) Saturn Kilometric Radiation (SKR) as observed by RPWS (presented as a flux density at 1AU). The data has been processed as explained by *Lamy et al.* [2008]. Below this, ENLIL solar wind conditions model results: (b) standoff distance of the magnetopause, (c) ram pressure, (d) the magnetic field strength and (e) velocity.

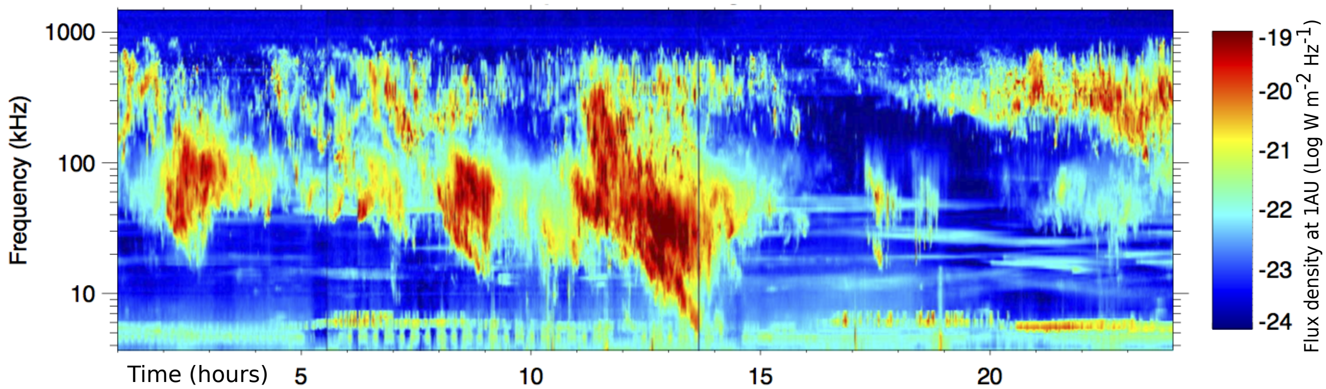

Figure D. Saturn kilometric radiation as observed by RPWS on the day of the cusp observation. On the x-axis is the universal time shown in hours. The data is presented as a flux density at 1AU (Log W m^{-2} Hz^{-1})